Supplemental Materials: Momentum-Resolved Observation of Thermal and Quantum Depletion in a Bose Gas

R. Chang, Q. Bouton, H. Cayla, C. Qu, A. Aspect, C. I. Westbrook and D. Clément

Production of gaseous condensates and detection after time-of-flight

Our condensates are produced in the 2^3S_1, $m_J = +1$ internal electronic state in a crossed dipole trap which is described in [15]. This metastable state has a lifetime of 8000 seconds. To measure the asymptotic momentum distribution $n_\infty(\mathbf{k})$ of the gas, we switch off the optical trap in 2 μs, allowing the cloud to undergo expansion while falling under the influence of gravity. The Micro-Channel Plate (MCP) detector and electronics are described in detail in [16]. The estimated detection efficiency is 25%. The spatial resolution in the plane of the detector is measured to be equal to $\simeq 100$ μm and the time resolution along the vertical axis is 10 μs.

The electronic detector is positioned 55 cm below the trapped gas giving a TOF value of 330 ms. To ensure that the gas expansion is un-perturbed by residual magnetic field gradients present during the TOF, atoms are transferred to the magnetically insensitive $m_J = 0$ state. This transfer is achieved with a radio-frequency (RF) which causes transitions between the magnetic sublevels whose energies have been split by a magnetic bias field with $\Delta E = E_{m_J=+1} - E_{m_J=0} \simeq h \times 10$ MHz. To transfer the atoms independently of their velocity, we use a RF sweep with central frequency 10 MHz and span of ± 500 kHz, applied on the atoms after a 2 ms TOF. The RF sweep is 1 ms long at constant RF power. After the RF sweep, we apply a magnetic gradient to push the atoms remaining in the $m_J = \pm 1$ states away from the detector. The RF power, combined with the removal of the $m_J = \pm 1$ states, allows us to control the flux of atoms ($m_J = 0$) striking the detector. We typically operate between 15 and 45% RF transfer efficiency (see **1D density profiles**). The scattering length in the $m_J = +1$ is $a_s^{m_J=+1} \simeq 142 a_0$, where a_0 is the Borh radius. In the $m_J = 0$ state, it has never been measured so we have inferred its value from the predictions of [27] with the knowledge of $a_s^{m_J=+1}$ to extract the contribution of the quintet potential. We find $a_s^{m_J=0} \sim 100 a_0$, much smaller than $a_s^{m_J=+1}$. Note that an experimental measurement might reveal corrections to this approximate value.

The MCP detector provides a three-dimensional histogram of atom numbers (see Fig. 1(b)). The position of an atom labelled with integer j is given by two-dimensional spatial coordinates (Y_j, Z_j) in the plane of the MCP and the time of arrival t_j. Similarly we note $(Y_0, Z_0, \bar{t} = t_0)$ the coordinates of the center of the cloud whose time of arrival defines the TOF $\bar{t}$ used throughout this work. In the frame centered on the falling could, the position $\mathbf{r}$ of the atom is $\mathbf{r} = (g\bar{t}/2t_j \times (\bar{t}^2 - t_j^2), Y_j - Y_0, Z_j - Z_0)$, accounting for the acceleration g of gravity. The use of the ballistic relation yields the asymptotic momentum distribution $n_\infty(\mathbf{k}) = (\hbar\bar{t}/m)^3\ n(\mathbf{r} = \hbar\mathbf{k}\bar{t}/m, \bar{t})$ (Eq. 1 in the main text). The momentum-space resolution is 0.03 μm^{-1} along directions y and z (in the MCP plane), and 0.01 μm^{-1} along x (orthogonal to the MCP plane). The distributions studied here consist of the the average of roughly 1500 experimental shots. Individual shots have been re-centered to account for slight fluctuations in cloud center-of-mass after the TOF.

The condensate atom number N_0 and density n_0 are calibrated by comparing the 3D density profiles on the MCP detector with the predictions of the scaling solution for our trap frequencies [19, 20]. The uncertainty on these values is evaluated to be 20%.

1D density profiles

From the three-dimensional asymptotic momentum density $n_\infty(\mathbf{k})$, one-dimensional profiles are generated for the radial and longitudinal cloud directions. Longitudinal profiles are cuts along the z direction (at $k_x \simeq k_y \simeq 0$) with a small integration along the two transverse x and y directions (see below). Radial profiles in the $x - y$ plane are generated from an angular average over azimuthal angles $|\phi| > 45°$, where $\phi = \arctan(k_x/k_y)$ (at $k_z \simeq 0$). This choice of azimuthal angles avoids a defect located on the surface of the micro-channel plate.

Since the experimental signals contain both a high-density condensate and low-density tails with a 4 decade separation in scales, it is necessary to divide the measurement of the density profile into two steps. To measure the condensate momentum components we first use a low RF transfer efficiency (typically 15%). In this low particle flux regime the MCP is far from electronic saturation, but the low-density tails are hard to detect. Secondly to measure the high-momentum tails, we use a high RF transfer efficiency (typically 45%). At high flux of detected particles, the dense condensate locally saturates the MCP, while the low-density wings remain unperturbed. We have verified that the two runs provide identical density profiles at intermediate k where local saturation is not a problem for the

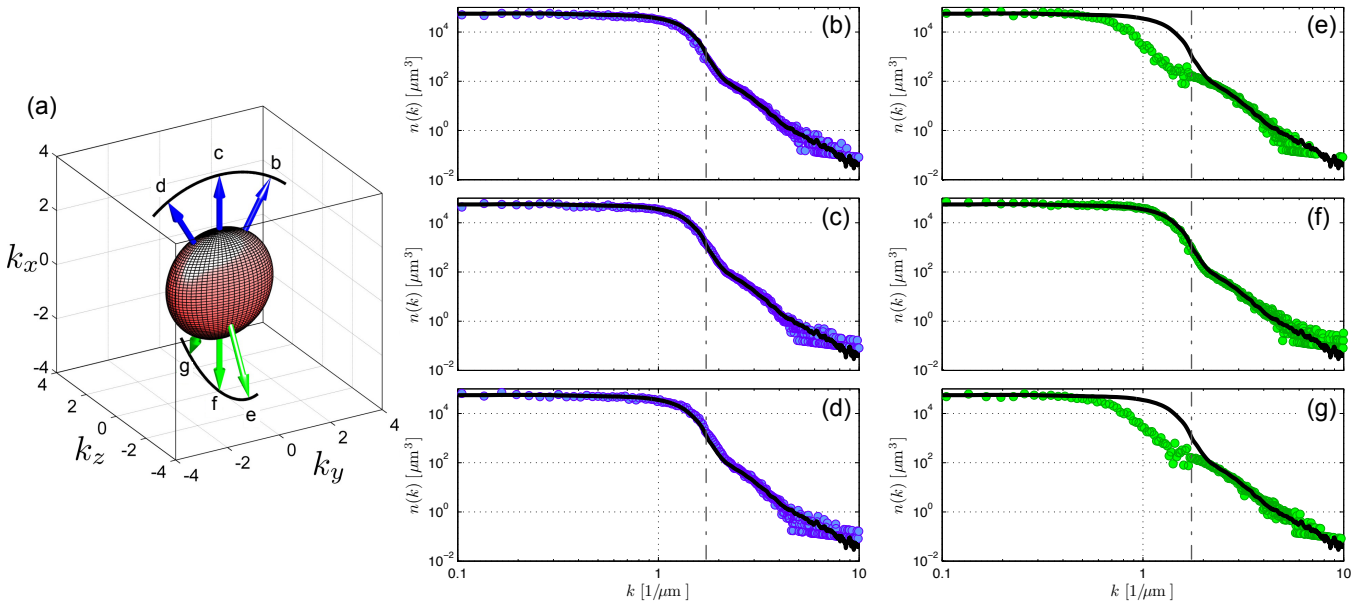

FIG. S1. Observed momentum distributions along various directions, showing the anisotropic condensate distribution and the isotropic components associated with the thermal and the quantum depletion. The vertical dot-dashed line delimits the condensate (low momenta k) and the condensate depletion. **(a)** Illustration of the anisotropic momentum distribution of the condensate in the far-field regime (pancake-shaped distribution). The arrows represent the directions along which we plot the 1D momentum profiles with a small angular average ($\pm 10^\circ$ degrees) in the panels (b)-(g). **(b)-(d)** Blue dots are the measured 1D momentum profiles in the $k_z = 0$ plane. **(e)-(g)** Green dots are the measured 1D momentum profiles in the $k_y = 0$ plane. In each subplot, the solid line is the radial 1D momentum profile plotted in Fig. 2 of the main text (obtained from a large angular average, see above).

high-flux runs and there is sufficient signal in the low-flux runs. The 1D profile for the condensate (low-flux data) has a transverse integration of $\pm$ 0.1 μm^{-1}. The profile for the tails (high-flux data) has transverse integration of $\pm$ 0.8 μm^{-1}. The two-step measurement and transverse integration ensures sufficient signal in the high-momentum tails, while accurately capturing the condensate profile at low-momenta.

In order to illustrate the observed symmetry in region **II** and **III**, we plot measured 1D profiles with a small angular average on ϕ ($\pm 10^\circ$ degrees) along different directions separated by 30°degrees in Fig. S1. The radial 1D profile shown in Fig. 2 (obtained from a large angular average) is reported as a black line in each subplot. The anisotropy of the condensate distribution appears clearly while the momentum profiles in region **II** and **III** have a spherical symmetry.

Mean-field momentum distribution of an interacting gas from time-of-flight

The condensate and its expansion is known to be well modeled by a mean-field interaction [3]. To verify that the observed tails (regions **II** and **III** in Fig. 2(b)) are not an artifact of the condensate, we compare our data to the complete 3D mean-field solution. The mean-field Gross-Pitaevskii (GP) solution beyond the Thomas-Fermi approximation may lead to the appearance of additional momentum components after TOF. These would result from slight modifications of the Thomas-Fermi real-space density occurring on the length scale $(a_{ho}^4/R)^{1/3}$, which fixes the characteristic thickness of the boundary [3] (here a_{ho} and R are, respectively, the oscillator length and the Thomas-Fermi radius and, for simplicity, we have assumed isotropic trapping).

The ground state is obtained by numerical simulation of the Gross-Pitaevskii equation in imaginary time, and the expansion dynamics are performed through real time propagation. The system size used in the calculations limits the simulated TOF. However, the distribution after 2.45 ms is observed to converge, indicating the complete conversion of mean-field interaction energy into kinetic energy. The numerical results for the distribution after a TOF of 2.45 ms are presented in Fig. S2, using the ballistic relation as defined in Eq. 1. The simulations clearly show that the mean-field Gross-Pitaevskii ground state is unable to reproduce the tails observed in the experiment.

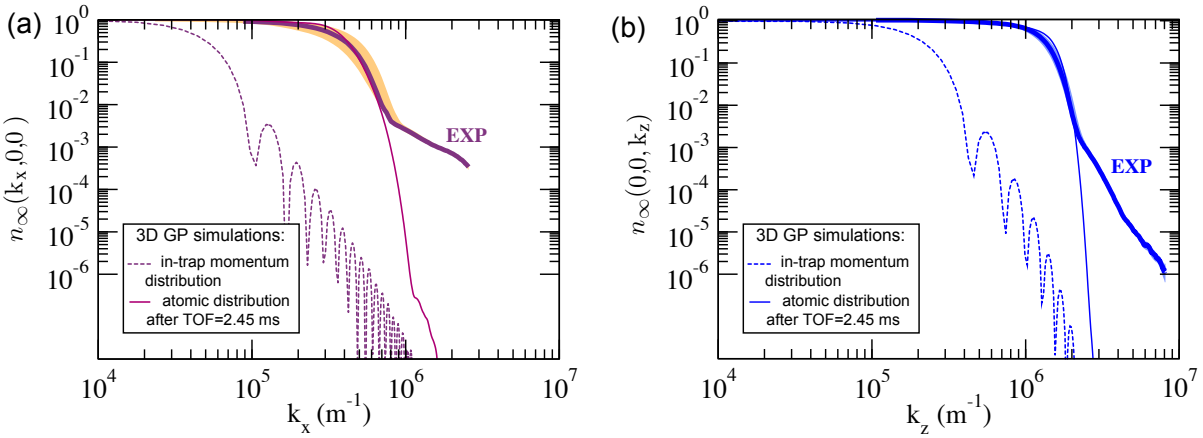

FIG. S2. Simulation of the expansion dynamics of a 3D Bose-Einstein condensate with the mean-field Gross-Pitaevskii equation. The parameters describing the condensate in the numerics (including atom number and trapping frequencies) are those of the experiment. The GP simulation is compared to the experimental data along the longitudinal **(a)** and radial **(b)** direction. It shows an excellent agreement in the region **I** associated with the condensate but does not reproduce the experimental tails. Numerical results and experimental distributions have been normalized to $n_\infty(0,0,0)=1$.

Quantum depletion with local density approximation at $T=0$

In uniform systems Bogoliubov's approach yields a population of momentum state equal to

$$n(k) = |v_k|^2 = \frac{\hbar^2k^2/2m + mc^2}{2\epsilon(k)} - \frac{1}{2} \tag{S1}$$

where $\epsilon(k) = \left[\hbar^2k^2c^2 + (\hbar^2k^2/2m)^2\right]^{1/2}$ is the Bogoliubov excitation spectrum. For a harmoncially trapped condensate in the Thomas-Fermi limit, the local speed of sound is $c(\mathbf{r}) = c_0\sqrt{1-(x/R_x)-(y/R_y)^2-(z/R_z)^2}$ with $c_0 = \sqrt{g_sn_0/m}$ the speed of sound at the trap center and $g_s = 4\pi\hbar^2a_s/m$. In the LDA one finds

$$n(\vec{k}) = \frac{1}{(2\pi)^3}\int |v_{\vec{k}}(\vec{r})|^2 d\vec{r} \tag{S2}$$

$$= \frac{R_xR_yR_z}{(2\pi)^2}\left[-\frac{13}{48} - \frac{5k^2\xi^2}{32} + \left(\frac{4+12k^2\xi^2+5k^4\xi^4}{32\sqrt{2}k\xi}\right)\arctan\left(\frac{\sqrt{2}}{k\xi}\right)\right] \tag{S3}$$

$$\underset{[k\xi\gg1]}{\simeq} \frac{R_xR_yR_z}{105\pi^2}\frac{1}{k^4\xi^4} \tag{S4}$$

where $\xi = \hbar/\sqrt{2}mc_0$ is the healing length.

Within the Bogoliubov approach in the LDA approximation, the Tan contact constant, defined as $\mathcal{C}/(2\pi)^3 = \lim_{k\to\infty}n(k)k^4$, is equal to $\mathcal{C}_{\rm LDA} = (64\pi^2/7)a_s^2N_0n_0$, with a_s the s-wave scattering length and N_0 (*resp.* n_0) the condensate atom number (*resp.* the condensate density). For metastable Helium, the calculation gives $(\mathcal{C}_{\rm LDA}/N_0)/n_0 \simeq 5.08\times10^{-15}$ m^{-2}.

Controlled heating sequence

To increase the temperature of our ultracold gas, we perform a controlled heating sequence using a 3D optical lattice. This sequence involves the adiabatic transfer of the gas from the optical dipole trap to the lattice in 30 ms, followed by a series of non-adiabatic lattice pulses of duration 0.5 ms during which the amplitude of the lattice is set to zero. The gas is then held in the optical lattice for 100 ms during which time it rethermalizes. Finally, we transfer the atom cloud adiabatically back to the initial optical dipole trap in 30 ms. Increasing the lattice depth while keeping the same sequence increases the final temperature of the gas at constant atom number and trapping frequencies.